
This is an electronic reprint of the original article.
This reprint may differ from the original in pagination and typographic detail.

Awan, Hafiz; Song, Zhanfeng; Saarakkala, Seppo E.; Hinkkanen, Marko
Optimal torque control of synchronous motor drives: plug-and-play method

Published in:
IEEE Energy Conversion Congress and Exposition, ECCE 2017

DOI:
[10.1109/ECCE.2017.8095801](https://doi.org/10.1109/ECCE.2017.8095801)

Published: 01/10/2017

Document Version
Peer-reviewed accepted author manuscript, also known as Final accepted manuscript or Post-print

Please cite the original version:
Awan, H., Song, Z., Saarakkala, S. E., & Hinkkanen, M. (2017). Optimal torque control of synchronous motor drives: plug-and-play method. In *IEEE Energy Conversion Congress and Exposition, ECCE 2017* (pp. 334-341). (IEEE Energy Conversion Congress and Exposition). IEEE. <https://doi.org/10.1109/ECCE.2017.8095801>

This material is protected by copyright and other intellectual property rights, and duplication or sale of all or part of any of the repository collections is not permitted, except that material may be duplicated by you for your research use or educational purposes in electronic or print form. You must obtain permission for any other use. Electronic or print copies may not be offered, whether for sale or otherwise to anyone who is not an authorised user.

Optimal Torque Control of Synchronous Motor Drives: Plug-and-Play Method

Hafiz Asad Ali Awan*, Zhanfeng Song†, Seppo E. Saarakkala*, and Marko Hinkkanen*

*Aalto University School of Electrical Engineering, Espoo, Finland

†Tianjin University School of Electrical and Information Engineering, Tianjin, China

Abstract—This paper deals with the optimal state reference calculation for synchronous motors with a magnetically salient rotor. A look-up table computation method for the maximum torque-per-ampere (MTPA), maximum torque-per-volt (MTPV), and field-weakening operation is presented. The proposed method can be used during the drive start-up, after the magnetic model identification. It is computationally efficient enough to be implemented directly in the embedded processor of the drive. For experimental validation, a 6.7-kW synchronous reluctance motor drive is used.

Index Terms—Field-weakening, look-up table, magnetically salient rotor, maximum torque-per-ampere, maximum torque-per-volt, optimal references, synchronous reluctance motor.

I. INTRODUCTION

Synchronous motors with a magnetically salient rotor—such as the interior permanent-magnet synchronous motor (IPM), the synchronous reluctance motor (SyRM), and the permanent-magnet (PM) assisted SyRM—are well suited for hybrid or electric vehicles, heavy-duty working machines, and industrial applications [1]–[6]. Depending on the operating speed and the torque reference, these drives are typically controlled to operate either at the maximum torque-per-ampere (MTPA) locus, in the field-weakening region, or at the maximum torque-per-volt (MTPV) limit. For this purpose, optimal current (or flux linkage) references should be determined as a function of the reference torque and operating speed. This calculation is typically done off-line and the resulting look-up tables are then used in the on-line control method.

The MTPA trajectory can be stored in a look-up table, which is either directly measured with a suitable test bench [7] or pre-computed based on the known saturation characteristics [1]. Alternatively, the MTPA locus can be tracked using signal injection [8]. The field-weakening methods can be broadly divided into feedback methods [9]–[12] and feed-forward methods [13]–[17]. The feedback methods apply the difference between the reference voltage and the maximum available voltage. These methods lead to maximum torque generation during the field-weakening operation, but they do not guarantee minimum losses. An additional voltage control loop is used, which has to be tuned and should have much lower bandwidth than the innermost current controller [11], [18]. Furthermore, a separate MTPV limit is needed also in the feedback methods.

Some feedforward field-weakening methods are based on analytical solutions of the intersection of the voltage ellipses and torque hyperbolas [13]. The disadvantage of these methods

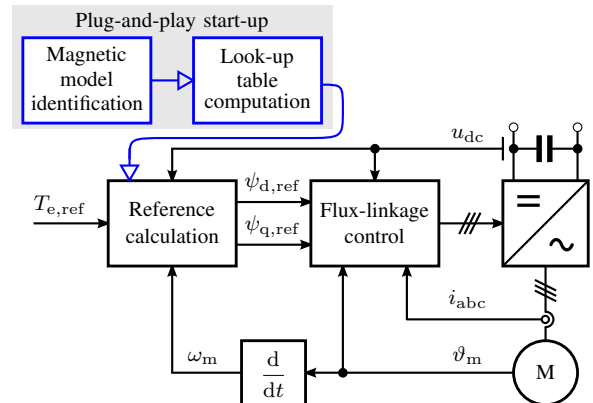


Fig. 1. Plug-and-play start-up method consists of two stages, magnetic model identification and look-up table computation, which can be run in the embedded processor of the drive. Look-up tables are then used in reference calculation. If needed, the current controller can be used instead of the flux-linkage controller.

is that they do not take the magnetic saturation into account (and the saturation effects cannot be properly taken into account afterwards, since the saturation deforms the shape of the voltage ellipses and torque hyperbolas). Other feedforward field-weakening methods are based on off-line calculated look-up tables [14]–[16], [19]. The magnetic saturation can properly be included in these methods, but the off-line data processing can be difficult and time-consuming, even though some open-source post-processing algorithms have recently become available [20].

Instead of current or flux linkage control, direct flux vector control can be used [17], [21]–[23]. In this method, the optimal references in the field-weakening region are easier to solve, but still the MTPA trajectory and the MTPV limit have to be implemented. A disadvantage of the direct flux vector control is that the inner control loops become nonlinear, which complicates their design.

In this paper, a plug-and-play method for the optimal torque control of synchronous motor is presented. The overall structure of the proposed approach is shown in Fig. 1. If needed, the proposed approach can be easily modified to use the current controller instead of the flux-linkage controller. The reference calculation block will need to be changed in such a way that the current references are generated instead of the flux references; the drawback is that two two-dimensional look-up tables are needed, one for the direct axis and the other for the

quadrature axis current component, as in [14], [15].

The proposed look-up table computation method can run in the embedded processor of the drive during the start-up, after the magnetic model of the motor has been identified. Alternatively, if the drive is connected to a cloud server or to a mobile phone, the look-up tables could be computed remotely and then uploaded to the drive. No additional user inputs or tunings are required and the drive is ready to be started.

The fundamental motor equations and magnetic model used are presented in Section II. Then, the main contributions of the paper are presented in Sections III and IV:

- 1) A systematic method for computing look-up tables for optimal current and flux linkage references is proposed. The look-up table computation method is combined with the magnetic model identification, making it a plug-and-play method as shown in Fig. 1.
- 2) A modified reference calculation scheme is proposed, using just one two-dimensional look-up table for the d-axis flux component. The q-axis flux component is obtained using the combination of the Pythagorean theorem and the bilinear interpolation.

In Section V, the proposed method is evaluated by means of the optimal characteristics, simulations, and experiments using a 6.7-kW SyRM drive.

II. MOTOR MODEL

The magnitude of the stator current is

$$i_s = \sqrt{i_d^2 + i_q^2} \quad (1)$$

where i_d and i_q are the current components. The magnitudes ψ_s and u_s of the stator flux and stator voltage, respectively, are obtained similarly.

A. Fundamental Equations

The motor model in rotor coordinates is considered. The stator voltage equations are

$$\frac{d\psi_d}{dt} = u_d - R_s i_d + \omega_m \psi_q \quad (2a)$$

$$\frac{d\psi_q}{dt} = u_q - R_s i_q - \omega_m \psi_d \quad (2b)$$

where i_d and i_q are the current components, ψ_d and ψ_q are the flux linkage components, u_d and u_q are the voltage components, ω_m is the electrical angular speed of the rotor, and R_s is the stator resistance. The current components

$$i_d = i_d(\psi_d, \psi_q) \quad i_q = i_q(\psi_d, \psi_q) \quad (3)$$

are generally nonlinear functions of the flux components. They are the inverse of the flux maps, often represented by two-dimensional look-up tables. Here, the modelling approach (3) is chosen, because it is more favourable towards representation in the algebraic form. Since the nonlinear inductor should not generate or dissipate electrical energy, the reciprocity condition [24]

$$\frac{\partial i_d}{\partial \psi_q} = \frac{\partial i_q}{\partial \psi_d} \quad (4)$$

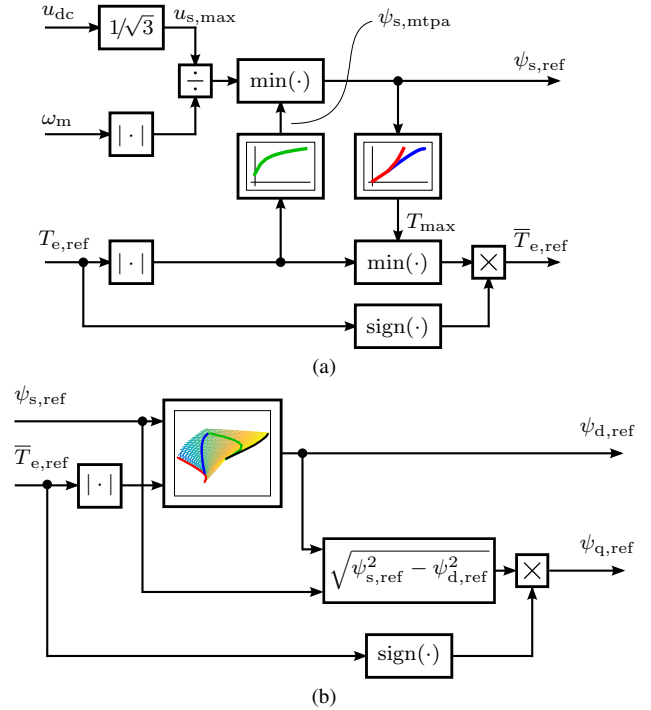


Fig. 2. Reference calculation: (a) stator flux magnitude $\psi_{s,ref}$ and limited torque reference $\bar{T}_{e,ref}$; (b) stator flux components $\psi_{d,ref}$ and $\psi_{q,ref}$. All three look-up tables can be computed during the start-up in the embedded processor of the drive using the identified algebraic magnetic model (6). The torque limit is $T_{max} = \min(T_{mtpv}, T_{lim})$, where T_{lim} is the limit corresponding to the maximum current magnitude.

should hold. Typically, the core losses are either omitted or modelled separately using a core-loss resistor in the model. The produced torque is

$$T_e = \frac{3p}{2} (\psi_d i_q - \psi_q i_d) \quad (5)$$

where p is the number of pole pairs. If the functions (3) and the stator resistance are known, the machine is fully characterized both in the steady and transient states. For example, the MTPA trajectory can be resolved from (3) and (5).

B. Algebraic Magnetic Model

To model the current components in (3), algebraic functions are used [25]

$$i_d = \left(a_{d0} + a_{dd} |\psi_d|^S + \frac{a_{dq}}{V+2} |\psi_d|^U |\psi_q|^{V+2} \right) \psi_d - i_f \quad (6a)$$

$$i_q = \left(a_{q0} + a_{qq} |\psi_q|^T + \frac{a_{dq}}{U+2} |\psi_d|^{U+2} |\psi_q|^V \right) \psi_q \quad (6b)$$

where a_{d0} , a_{dd} , a_{q0} , a_{qq} , and a_{dq} are nonnegative coefficients and S , T , U , and V are nonnegative exponents. The constant i_f models the magnetomotive force due to the permanent magnets. In both functions given in (6), the first two terms in parenthesis correspond to the self-axis characteristics and the last term models the cross-saturation. The form of the last term originates from the reciprocity condition (4), which is satisfied. The model is invertible: for any given values of i_d

TABLE I
FITTED PARAMETERS FOR A 6.7-kW SYRM GIVEN IN SI UNITS

S	T	U	V	a_{d0}	a_{dd}	a_{q0}	a_{qq}	a_{dq}	i_f
1	5	0	1	52.0	658.6	17.3	369.5	1121.7	0

TABLE II
FITTED PARAMETERS FOR A 7.7-kW PM-SYRM GIVEN IN SI UNITS

S	T	U	V	a_{d0}	a_{dd}	a_{q0}	a_{qq}	a_{dq}	i_f
0	5	0	0	304.0	0	32.1	2084.3	0	35.4

and i_q , the corresponding values of ψ_d and ψ_q can be obtained by numerically solving (6).

The parameters of the magnetic model for a 6.7-kW SyRM are given in Table I and for a 7.7-kW PM-SyRM in Table II. The d-axis is selected along the minimum inductance axis. For SyRMs, a self-identification method for the magnetic model in (6) is available [25].

III. CONTROL SCHEME

Fig. 1 depicts the overall structure of the control system. Fig. 2 shows the reference calculation scheme. As shown in Fig. 2(a), the optimal MTPA flux magnitude $\psi_{s,\text{mtpa}}$ is read from a look-up table, whose input is the torque reference. The MTPA flux is limited based on the maximum available voltage $u_{s,\text{max}}$, yielding the optimal flux magnitude $\psi_{s,\text{ref}}$ under the voltage constraint. The maximum voltage $u_{s,\text{max}}$ is calculated from the measured DC-link voltage u_{dc} . Hence, any sudden variations in u_{dc} are directly translated into the references.

The torque reference is limited by the torque T_{max} corresponding to the combined MTPV and current limit, yielding the limited torque reference $\bar{T}_{e,\text{ref}}$. The limit T_{max} is read from the look-up table, whose input is the optimal flux magnitude $\psi_{s,\text{ref}}$. The benefit of the scheme in Fig. 2(a) is that whatever the input torque reference $T_{e,\text{ref}}$ and the speed ω_m are, the optimal values $\psi_{s,\text{ref}}$ and $\bar{T}_{e,\text{ref}}$ are obtained without any delays. It should be noted that the scheme shown in Fig. 2(a) can also be used directly in combination with the direct flux vector control.

As shown in Fig. 2(b), a two-dimensional look-up table is used to determine $\psi_{d,\text{ref}}$ based on the optimal references $\psi_{s,\text{ref}}$ and $\bar{T}_{e,\text{ref}}$. Bilinear interpolation is used to get the value of $\psi_{d,\text{ref}}$ from the two-dimensional look-up table. Generally, four points are needed for the bilinear interpolation. The data is not available for the two-dimensional look-up table beyond the MTPV limit. So, when operating along the MTPV limit, there are only three points available for the interpolation algorithm. The procedure to calculate the value of $\psi_{d,\text{ref}}$ using both the three and four points is given in the Appendix.

The value of the q-axis flux component $\psi_{q,\text{ref}}$ can be calculated from the final interpolated result $\psi_{d,\text{ref}}$ using the Pythagorean theorem, but it will create chattering close to zero torque in the calculated references. Instead, the q-axis flux component is first calculated using the Pythagorean theorem at

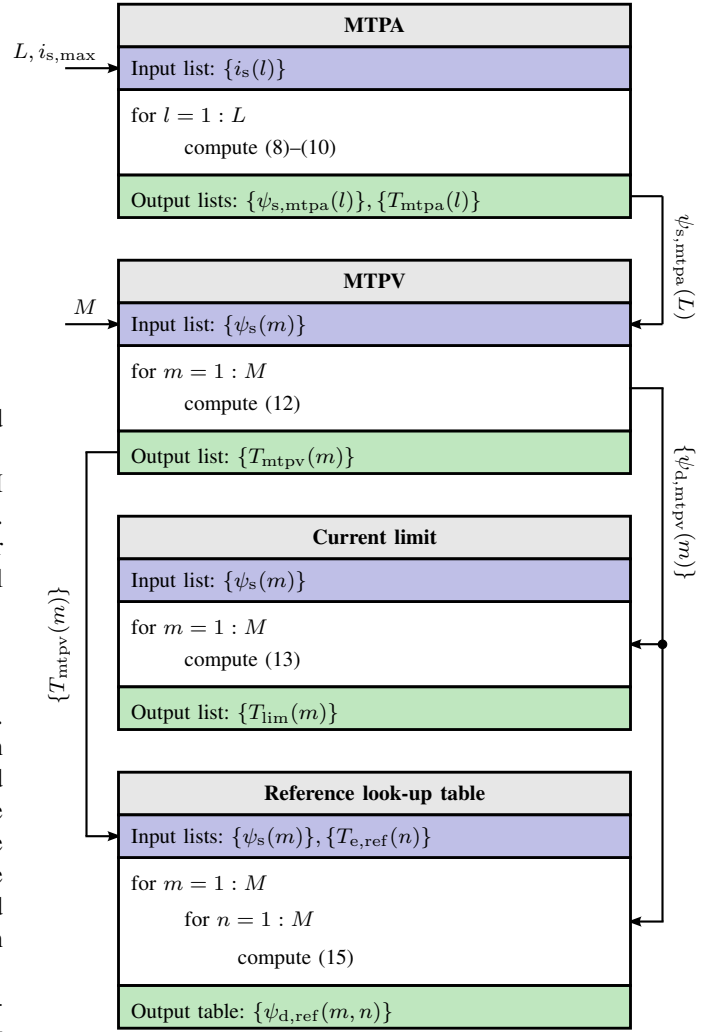


Fig. 3. Look-up table computation procedure. The parameters of the magnetic model (6) are also needed in each stage.

all the (three or four) points used in the interpolation algorithm for $\psi_{d,\text{ref}}$ and then $\psi_{q,\text{ref}}$ is obtained using the bilinear interpolation. Further details about the used interpolation method are given in the Appendix.

Finally, if needed, the flux references can be transformed into the current references using the algebraic magnetic model (6). If the current references are calculated directly from the optimal references $\psi_{s,\text{ref}}$ and $\bar{T}_{e,\text{ref}}$, two two-dimensional look-up tables are needed [14]–[16].

IV. LOOK-UP TABLE COMPUTATION

Fig. 3 shows an overall diagram of the look-up table computation method, which is divided into four stages. In the following equations, the d-axis of the coordinate system is fixed to the direction of the permanent magnets (or along the minimum inductance axis), without loss of generality. After the look-up table computation, the d- and q-axes of the SyRM are flipped to the standard SyRM representation, i.e., the d-axis along the maximum inductance axis.

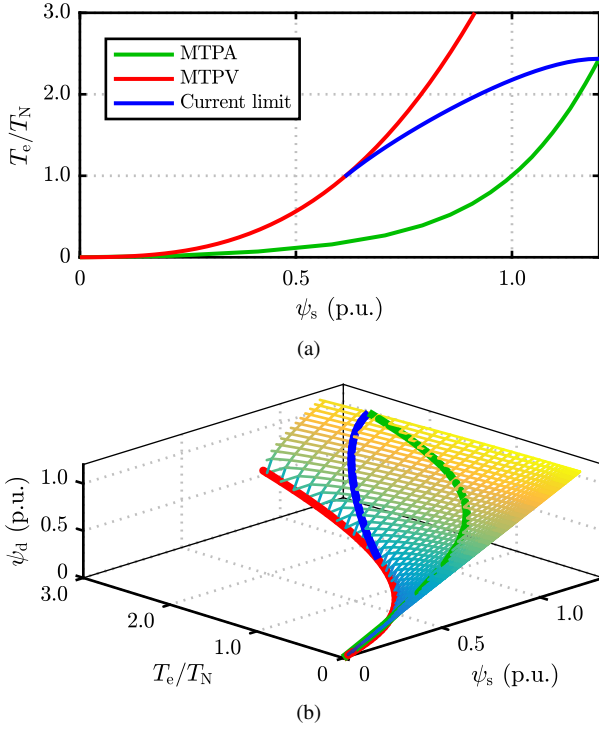


Fig. 4. Look-up tables for a 6.7-kW SyRM: (a) MTPA locus, MTPV limit, and current limit; (b) ψ_d . The feasible operating region in ψ_d plot is limited by the MTPA locus, MTPV limit, and current limit, which are also plotted. These look-up tables are applied in the controller according to Fig. 2. T_N is the rated torque of the motor. For illustration purposes, $L = 20$ and $M = 50$ is used in these plots.

It is to be noted that the method is not limited to the saturation model (6). Different magnetic models or even look-up tables could be used instead, if they are physically feasible and invertible in the relevant operation range. Furthermore, the reference calculation scheme shown in Fig. 2 is used as an example in this paper, but the proposed look-up table computation method can be easily modified for other reference calculation schemes and control structures as well.

A. MTPA

For creating a look-up table, a list of L equally-spaced current magnitudes is defined

$$\{i_s(l)\} = (l-1)\Delta i, \quad l = 1, 2, \dots, L \quad (7)$$

where $\Delta i = i_{s,\max}/(L-1)$ and $i_{s,\max}$ is the maximum current. For each current magnitude i_s , the maximum torque T_{mtpa} and the corresponding argument $i_{d,\text{mtpa}}$ are obtained by solving the optimization problem

$$T_{\text{mtpa}} = \max_{i_d \in [-i_s, 0]} T_e(i_d) \quad (8a)$$

where the torque is expressed as a function of i_d

$$T_e(i_d) = \frac{3p}{2} [\psi_d(i_d, i_q) \cdot i_q(i_d) - \psi_q(i_d, i_q) \cdot i_d] \quad (8b)$$

$$i_q(i_d) = \sqrt{i_s^2 - i_d^2} \quad (8c)$$

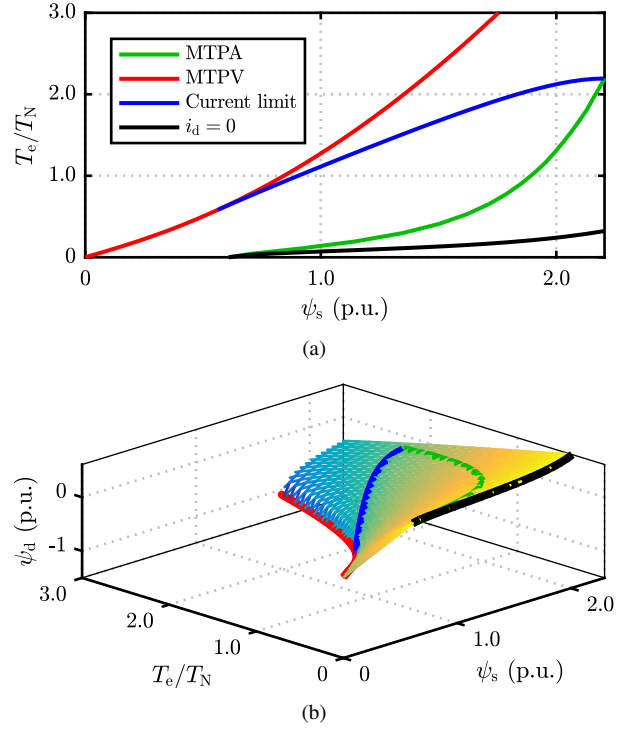


Fig. 5. Look-up tables for a 7.7-kW PM-SyRM: (a) MTPA locus, MTPV limit, current limit, and $i_d = 0$ line; (b) ψ_d . Look-up tables are not calculated beyond $i_d = 0$ line.

and the search interval is $-i_s \leq i_d \leq 0$. The flux components ψ_d and ψ_q corresponding to i_d and i_q are calculated by numerically inverting the algebraic magnetic model (6), i.e.,

$$(\psi_d, \psi_q) = \text{solve}_{\psi_d, \psi_q} \begin{cases} i_d(\psi_d, \psi_q) = i_d \\ i_q(\psi_d, \psi_q) = i_q \end{cases} \quad (9)$$

After solving (8), the optimal q-component $i_{q,\text{mtpa}}$ is obtained from (8c).

The optimal flux magnitude is

$$\psi_{s,\text{mtpa}} = \sqrt{\psi_{d,\text{mtpa}}^2 + \psi_{q,\text{mtpa}}^2} \quad (10)$$

where $\psi_{d,\text{mtpa}}$ and $\psi_{q,\text{mtpa}}$ corresponding to $i_{d,\text{mtpa}}$ and $i_{q,\text{mtpa}}$ are obtained using (9). The Brent algorithm [26] is used for solving (8) without using derivatives. The Powell dogleg algorithm [27] is used for inverting the magnetic model in (9).

As shown in Fig. 3, the procedure (8)–(10) is repeated in a *for* loop for each element $i_s(l)$ of the list (7). Then, a look-up table for the control system, cf. Fig. 2, is created from the resulting lists $\{\psi_{s,\text{mtpa}}(l)\}$ and $\{T_{\text{mtpa}}(l)\}$. As illustrated in Fig. 3, the inputs to the MTPA computation stage are the number of points L to be computed, the maximum current $i_{s,\max}$, and the parameters of the magnetic model (6). The maximum current $i_{s,\max}$ is selected based on the motor and converter ratings. Typically, L around 10 suffices.

Fig. 4(a) shows the computed MTPA look-up table for the 6.7-kW SyRM and Fig. 5(a) for the 7.7-kW PM-SyRM. In the

control algorithm, the optimal flux reference magnitude $\psi_{s,\text{ref}}$ is obtained based on this look-up table, as shown in Fig. 2(a).

B. MTPV

For creating the look-up table, a list of M equally-spaced stator flux magnitudes is defined

$$\{\psi_s(m)\} = (m-1)\Delta\psi, \quad m = 1, 2, \dots, M \quad (11)$$

where $\Delta\psi = \psi_{s,\text{max}}/(M-1)$ and the maximum flux magnitude $\psi_{s,\text{max}} = \psi_{s,\text{mtpa}}(L)$ is the result from the last step of the MTPA computation. For each flux magnitude ψ_s , the maximum torque T_{mtpv} is obtained by solving

$$T_{\text{mtpv}} = \max_{\psi_d \in [-\psi_s, 0]} T_e(\psi_d) \quad (12a)$$

where the torque is expressed as

$$T_e(\psi_d) = \frac{3p}{2} [\psi_d \cdot i_q(\psi_d, \psi_q) - \psi_q(\psi_d) \cdot i_d(\psi_d, \psi_q)] \quad (12b)$$

$$\psi_q(\psi_d) = \sqrt{\psi_s^2 - \psi_d^2} \quad (12c)$$

The magnetic model (6) is directly used in (12b), i.e., no magnetic model inversion is needed in this stage. The Brent algorithm is used for solving the optimization problem (12).

As shown in Fig. 3, the problem (12) is solved for each element $\psi_s(m)$ of the list (11). Then, a look-up table for the control system is created using the resulting output list $\{T_{\text{mtpv}}(m)\}$. Figs. 4(a) and 5(a) show the computed MTPV look-up tables for the two machines.

C. Maximum Current Limit

The already defined input list (11) of the flux magnitudes is considered. For each flux magnitude $\psi_s(m)$, the d-component $\psi_{d,\text{lim}}$ of the flux corresponding to the maximum current $i_{s,\text{max}}$ is solved

$$\psi_{d,\text{lim}} = \text{solve}_{\psi_d \in [\psi_{d,\text{mtpv}}, \psi_{d,\text{max}}]} \{i_s^2(\psi_d) = i_{s,\text{max}}^2\} \quad (13a)$$

where the square of the current magnitude is expressed as

$$i_s^2(\psi_d) = i_d^2(\psi_d, \psi_q) + i_q^2(\psi_d, \psi_q) \quad (13b)$$

$$\psi_q(\psi_d) = \sqrt{\psi_s^2 - \psi_d^2} \quad (13c)$$

The lower bound $\psi_{d,\text{mtpv}}$ in (13) is the d-component of the MTPV flux at each ψ_s and the upper bound $\psi_{d,\text{max}}$ is the d-component of the MTPA flux at the maximum current. After (13) has been solved, the corresponding torque T_{lim} is obtained from (12b). The Brent algorithm is used to solve this bounded nonlinear problem.

As shown in Fig. 3, the problem (13) is solved for each element $\psi_s(m)$. The lower bounds $\{\psi_{d,\text{mtpv}}(m)\}$ needed in (13) have already been computed during the MTPV stage. The upper bound $\psi_{d,\text{max}} = \psi_{d,\text{mtpa}}(L)$ is the d-component of the MTPA flux at the maximum current $i_{s,\text{max}}$ and it has also been computed. From the resulting output list $\{T_{\text{lim}}(m)\}$, a look-up table for the control system is created. Figs. 4(a) and 5(a) show the computed current limits of two times the rated

current for the SyRM and PM-SyRM. The MTPV and current limits can be easily merged into one limit

$$T_{\text{max}} = \min(T_{\text{mtpv}}, T_{\text{lim}}). \quad (14)$$

D. Two-Dimensional Reference Look-Up Table

For given flux magnitude ψ_s and torque reference $T_{e,\text{ref}}$, the d-component $\psi_{d,\text{ref}}$ is solved

$$\psi_{d,\text{ref}} = \text{solve}_{\psi_d \in [\psi_{d,\text{mtpv}}, \psi_s]} \{T_{e,\text{ref}} = T_e(\psi_d)\} \quad (15)$$

where the torque $T_e(\psi_d)$ is given by (12b). The lower bound $\psi_{d,\text{mtpv}}$ is the d-component of the MTPV flux at ψ_s . The Brent algorithm is used to solve (15).

For creating the look-up table, (15) can be solved in two nested *for* loops. As an input to one loop, the list (11) of the flux magnitudes $\{\psi_s(m)\}$ is used. In the other loop, the already calculated MTPV torque values $\{T_{\text{mtpv}}(m)\}$ can be used as an input, i.e. $\{T_{e,\text{ref}}(n)\} = \{T_{\text{mtpv}}(m)\}$. This selection not only defines the maximum torque which can be generated (under the MTPV limit) but also explicitly gives the lower bound $\psi_{d,\text{mtpv}}$ for each $\psi_{d,\text{ref}}$. If the maximum current is fixed, $\{T_{e,\text{ref}}(n)\} = \{T_{\text{max}}(m)\}$ can be used instead. The look-up table for the control system is created from the resulting table $\{\psi_{d,\text{ref}}(m, n)\}$. Figs. 4(b) and 5(b) show the two-dimensional look-up tables for the two machines. The $i_d = 0$ line shown in Fig. 5 does not need to be computed, but it is shown just for illustration purposes.

V. RESULTS

The computed look-up tables and the reference calculation scheme shown in Fig. 2 were evaluated by means of the optimal characteristics, simulations, and experiments. The parameters used for the look-up table computation are: $L = 10$; $M = 150$; and $i_{s,\text{max}} = 2$ p.u. The parameters of the magnetic model (6) given in Tables I and II are also needed. The computation time for the proposed method is less than 35 s in an Android phone. We expect the computation time to be slightly longer in typical digital-signal processors applied in frequency converters.

The rated values of the 6.7-kW four-pole SyRM are: speed 3175 r/min; frequency 105.8 Hz; line-to-line rms voltage 370 V; rms current 15.5 A; and torque 20.1 Nm. The rated values of the 7.7-kW four-pole PM-SyRM are: speed 3000 r/min; frequency 100 Hz; line-to-line rms voltage 147 V; rms current 17.7 A; and torque 24 Nm.

A. Optimal Characteristics

The effect of the magnetic saturation on the optimal current references in the i_d - i_q plane and on the optimal flux references in the ψ_d - ψ_q plane for the two motors is illustrated in Figs. 6 and 7. The solid curves correspond to the calculated optimal values, while the magnetic saturation is omitted in the case of the dashed curves. The effects of saturation are clearly visible; using constant inductances would result in a selection of non-optimal operating points.

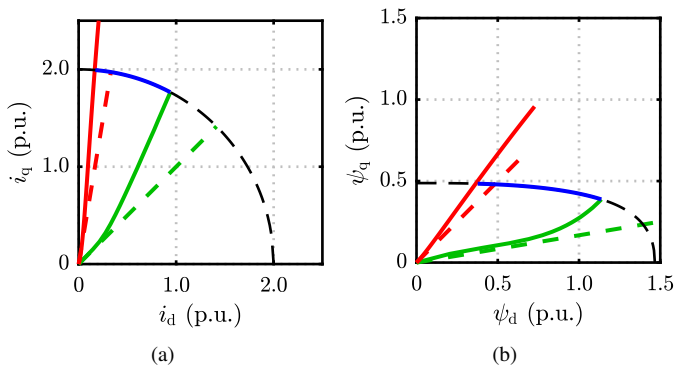


Fig. 6. MTPA, MTPV, and current limit control trajectories for the 6.7-kW SyRM: (a) i_d - i_q plane; (b) ψ_d - ψ_q plane. The dashed lines show the results, when the magnetic saturation is not taken into account (inductances correspond to the rated operating point). The black dashed curve corresponds to the constant current circle.

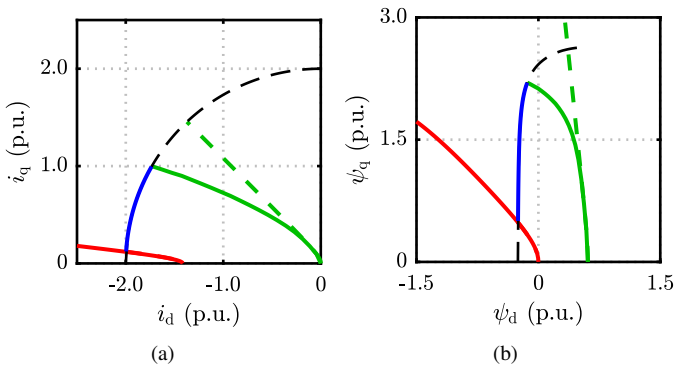


Fig. 7. MTPA, MTPV, and current limit control trajectories for the 7.7-kW PM-SyRM: (a) i_d - i_q plane; (b) ψ_d - ψ_q plane.

The effect of the magnetic saturation on the torque generation is illustrated in Fig. 8. The torque generated in the case when the magnetic saturation is included in the reference calculation is compared to the case when the magnetic saturation is omitted. It can be seen that the torque generated in the saturated case is much higher than the unsaturated case.

Fig. 9 shows the torque versus speed curve for different current limits. If needed, the reference calculation scheme in Fig. 2(a) can be modified easily to use multiple current limits or even a dynamic current limit, as needed in some industrial applications. The only difference will be using multiple one-dimensional current limit look-up tables. Three to four one-dimensional look-up tables could be used for different current limits and then the results between these limits could be interpolated as required.

B. Simulations

Simulations and experiments were performed on a 6.7-kW SyRM drive. The magnetic saturation in the motor model and the controller is modelled using the magnetic model in (6). The load torque coming from the viscous friction acting on the system is modelled as $T_L = b\omega_m$, where $b = 0.0014$ Nms

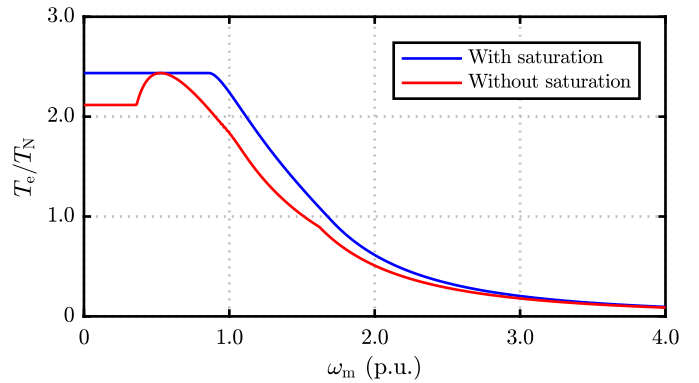


Fig. 8. Torque vs speed curve for the SyRM generated from the reference calculation block with and without taking magnetic saturation into account. Rated inductance values are used for the unsaturated case. The current limit was set to 2 p.u.

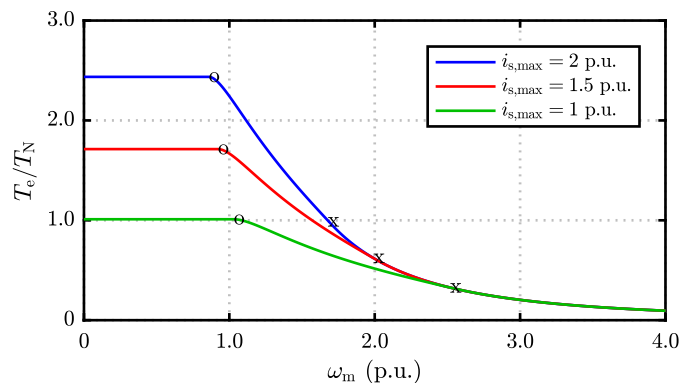


Fig. 9. Torque vs speed curve for the SyRM generated from the reference calculation block for different current limits, where $i_{s,max}$ is the maximum current magnitude. The onset of the field-weakening in each case is depicted by a circle and the MTPV limit by a cross.

is the coefficient of the viscous friction. The total moment of inertia is 0.03 kgm².

Fig. 10 shows the acceleration test for the 6.7-kW SyRM. The motor is accelerated from zero to 2-p.u. speed. The current limit was set to 2 p.u. in the calculated look-up tables. From the last subplot in Fig. 10, it can be seen that the measured current is slightly higher than the 2-p.u. limit at $t \approx 0.9$ s. This error could be reduced by decreasing the mesh size of the two-dimensional look-up table $\psi_d(\psi_s, T_e)$, i.e., by increasing the value of M in look-up table computation.

C. Experiments

The reference calculation scheme shown in Fig. 2 was experimentally evaluated together with the calculated look-up tables. The controller was implemented in an OPAL-RT OP5600 rapid-prototyping system. The rotor speed ω_m is measured using an incremental encoder. The stator currents and the DC-link voltage are measured. A discrete-time flux-linkage controller was used [19].

As an example, Fig. 11 shows the results for a speed reference step of 2 p.u. It can be seen that the measurement results follow the simulation results in Fig. 10, apart from

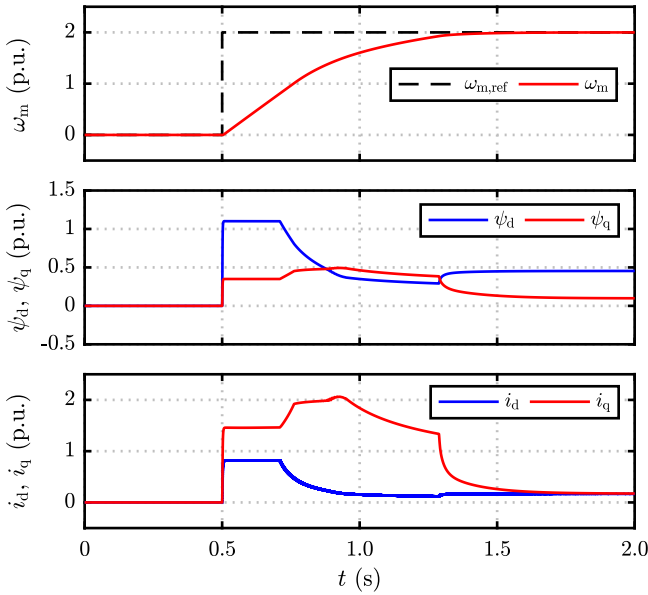


Fig. 10. Simulation results for the 6.7-kW SyRM: speed reference is stepped from zero to 2 p.u. The first subplot shows the reference speed $\omega_{m,\text{ref}}$ and the actual speed ω_m . The second subplot shows the flux components ψ_d and ψ_q . The last subplot shows the measured current components i_d and i_q .

the noise in current waveforms. The noise in the current waveforms is generated from the highly nonlinear saturation characteristics and spatial inductance harmonics of the SyRM.

VI. CONCLUSIONS

The optimal state reference calculation and the look-up table computation method for the MTPA, MTPV, and field-weakening operation is presented. The developed method could be used during the commissioning stage of the drive and it only needs to run once during the lifetime of the drive. The importance of including the magnetic saturation when calculating the state references is highlighted. The magnetic saturation cannot be included after the references have been calculated. Using constant inductances would result in a selection of non-optimal operating points, as the saturation deforms the voltage ellipses and torque hyperbolas. The proposed method properly takes the magnetic saturation into account, when calculating the state references. The computed look-up tables and the reference calculation scheme were evaluated using experiments on a 6.7-kW SyRM drive.

APPENDIX INTERPOLATION

If the value of the flux ψ_d is available at four points (coming from the two-dimensional look-up table) as shown in Fig. 12, then the value of $\psi_{d,\text{ref}} = f_d(x, y)$ is given by

$$f_d(x, y) = \frac{1}{(x_2 - x_1)(y_2 - y_1)} \begin{bmatrix} x_2 - x & x - x_1 \\ f_d(x_1, y_1) & f_d(x_1, y_2) \\ f_d(x_2, y_1) & f_d(x_2, y_2) \end{bmatrix} \begin{bmatrix} y_2 - y & y - y_1 \end{bmatrix} \quad (16)$$

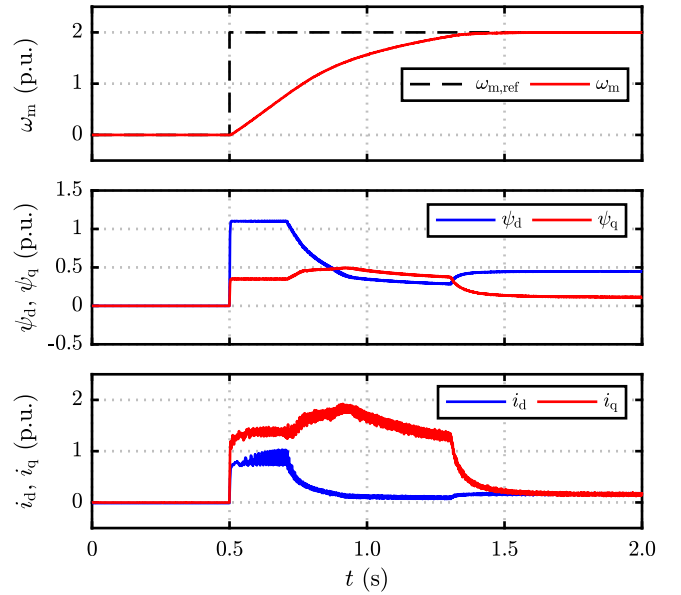


Fig. 11. Experimental results for the 6.7-kW SyRM: speed reference is stepped from zero to 2 p.u.

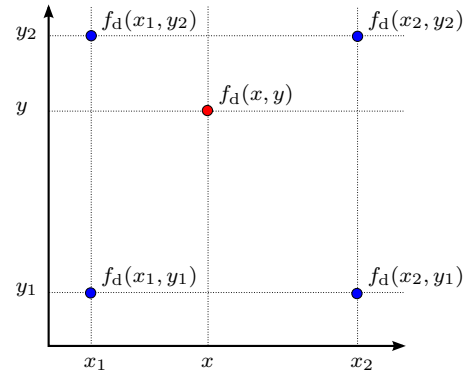


Fig. 12. Interpolation when the values of the function f_d are available on four points. The x -axis represents the flux reference $\psi_{s,\text{ref}}$ and y -axis the torque reference $T_{e,\text{ref}}$.

There is no data available for the two-dimensional look-up table $\psi_d(\psi_s, T_e)$ beyond the MTPV limit. When operating along the MTPV limit, there are only three points where the data is available. So, (16) cannot be used to interpolate the value of $\psi_{d,\text{ref}}$.

If one of the points, e.g., $f_d(x_2, y_1)$ is not available, then the remaining three points can be used to interpolate the value of the function $f_d(x, y)$ by a plane equation

$$f_d(x, y) = ax + by + c \quad (17)$$

where

$$\begin{bmatrix} a \\ b \\ c \end{bmatrix} = \begin{bmatrix} x_1 & y_1 & 1 \\ x_1 & y_2 & 1 \\ x_2 & y_2 & 1 \end{bmatrix}^{-1} \begin{bmatrix} f_d(x_1, y_1) \\ f_d(x_1, y_2) \\ f_d(x_2, y_2) \end{bmatrix}$$

To get the value of $\psi_{q,\text{ref}}$, first the value of ψ_q is calculated using the Pythagorean theorem at all the given points shown

in Fig. 12. Depending on whether four or three points are available, $\psi_{q,\text{ref}} = f_q(x, y)$ can be calculated using (16) or (17).

ACKNOWLEDGMENT

The work was supported in part by ABB Oy and in part by the Academy of Finland.

REFERENCES

- [1] T. M. Jahns, G. B. Kliman, and T. W. Neumann, "Interior permanent-magnet synchronous motors for adjustable-speed drives," *IEEE Trans. Ind. Appl.*, vol. IA-22, no. 4, pp. 738–747, July 1986.
- [2] W. L. Soong and T. J. E. Miller, "Field-weakening performance of brushless synchronous AC motor drives," *IEE Proc. Electr. Power Appl.*, vol. 141, no. 6, pp. 331–340, Nov. 1994.
- [3] Z. Q. Zhu and D. Howe, "Electrical machines and drives for electric, hybrid, and fuel cell vehicles," *Proc. of the IEEE*, vol. 95, no. 4, pp. 746–765, Apr. 2007.
- [4] S. Morimoto, Y. Takeda, T. Hirasaka, and K. Taniguchi, "Expansion of operating limits for permanent magnet motor by current vector control considering inverter capacity," *IEEE Trans. Ind. Appl.*, vol. 26, no. 5, pp. 866–871, Sept./Oct. 1990.
- [5] G. Pellegrino, A. Vagati, B. Boazzo, and P. Guglielmi, "Comparison of induction and PM synchronous motor drives for EV application including design examples," *IEEE Trans. Ind. Appl.*, vol. 48, no. 6, pp. 2322–2332, Nov. 2012.
- [6] N. Bianchi, S. Bolognani, E. Carraro, M. Castiello, and E. Fornasiero, "Electric vehicle traction based on synchronous reluctance motors," *IEEE Trans. Ind. Appl.*, vol. 52, no. 6, pp. 4762–4769, Nov. 2016.
- [7] I. Jeong, B.-G. Gu, J. Kim, K. Nam, and Y. Kim, "Inductance estimation of electrically excited synchronous motor via polynomial approximations by least square method," *IEEE Trans. Ind. Appl.*, vol. 51, no. 2, pp. 1526–1537, Mar. 2013.
- [8] S. Kim, Y.-D. Yoon, S.-K. Sul, and K. Ide, "Maximum torque per ampere (MTPA) control of an IPM machine based on signal injection considering inductance saturation," *IEEE Trans. Power Electron.*, vol. 28, no. 1, pp. 488–497, Jan. 2013.
- [9] J.-M. Kim and S.-K. Sul, "Speed control of interior permanent magnet synchronous motor drive for the flux weakening operation," *IEEE Trans. Ind. Appl.*, vol. 33, no. 1, pp. 43–48, Jan. 1997.
- [10] L. Harnefors, K. Pietiläinen, and L. Gertmar, "Torque-maximizing field-weakening control: design, analysis, and parameter selection," *IEEE Trans. Ind. Electron.*, vol. 48, no. 1, pp. 161–168, Feb. 2001.
- [11] N. Bedetti, S. Calligaro, and R. Petrella, "Analytical design of flux-weakening voltage regulation loop in IPMSM drives," in *Proc. ECCE'15*, Montreal, Canada, Sept. 2015, pp. 6145–6152.
- [12] P.-Y. Lin, W.-T. Lee, S.-W. Chen, J.-C. H., and Y.-S. Lai, "Infinite speed drives control with MTPA and MTPV for interior permanent magnet synchronous motor," in *Proc. IEEE IECON'14*, Dallas, TX, Oct. 2014, pp. 668–674.
- [13] S.-Y. Jung, J. Hong, and K. Nam, "Current minimizing torque control of the IPMSM using Ferrari's method," *IEEE Trans. Power Electron.*, vol. 28, no. 12, pp. 5603–5617, Dec. 2013.
- [14] M. Meyer and J. Böcker, "Optimum control for interior permanent magnet synchronous motors (IPMSM) in constant torque and flux weakening range," in *Proc. EPE-PEMC 2006*, Portoroz, Slovenia, Aug./Sept. 2006, pp. 282–286.
- [15] W. Peters, O. Wallscheid, and J. Böcker, "Optimum efficiency control of interior permanent magnet synchronous motors in drive trains of electric and hybrid vehicles," in *Proc. EPE'15 ECCE-Europe*, Geneva, Switzerland, Sept. 2015, pp. 1–10.
- [16] T. Huber, W. Peters, and J. Böcker, "Voltage controller for flux weakening operation of interior permanent magnet synchronous motor in automotive traction applications," in *Proc. IEMDC'15*, Coeur d'Alene, ID, May 2015, pp. 1078–1083.
- [17] G. Pellegrino, R. I. Bojoi, and P. Guglielmi, "Unified direct-flux vector control for ac motor drives," *IEEE Trans. Ind. Appl.*, vol. 47, no. 5, pp. 2093–2102, Sept. 2011.
- [18] L. Harnefors, "Design and analysis of general rotor-flux-oriented vector control systems," *IEEE Trans. Ind. Electron.*, vol. 48, no. 2, pp. 383–390, Apr. 2001.
- [19] H. A. A. Awan, T. Tuovinen, S. E. Saarakkala, and M. Hinkkanen, "Discrete-time observer design for sensorless synchronous motor drives," *IEEE Trans. Ind. Appl.*, vol. 52, no. 5, pp. 3968–3979, Sept. 2016.
- [20] Synchronous reluctance (machines) - evolution. [Online]. Available: <https://sourceforge.net/projects/syr-e/>
- [21] G. Pellegrino, E. Armando, and P. Guglielmi, "Direct-flux vector control of IPM motor drives in the maximum torque per voltage speed range," *IEEE Trans. Ind. Electron.*, vol. 59, no. 10, pp. 3780–3788, Oct. 2012.
- [22] G. Pellegrino, B. Boazzo, and T. Jahns, "Plug-in direct-flux vector control of PM synchronous machine drives," *IEEE Trans. Ind. Appl.*, vol. 51, no. 5, pp. 3848–3857, Sept. 2015.
- [23] B. Boazzo and G. Pellegrino, "Model-based direct flux vector control of permanent-magnet synchronous motor drives," *IEEE Trans. Ind. Appl.*, vol. 51, no. 4, pp. 3126–3136, July 2015.
- [24] A. Vagati, M. Pastorelli, F. Scapino, and G. Franceschini, "Impact of cross saturation in synchronous reluctance motors of the transverse-laminated type," *IEEE Trans. Ind. Appl.*, vol. 36, no. 4, pp. 1039–1046, Jul./Aug. 2000.
- [25] M. Hinkkanen, P. Pescetto, E. Molsa, S. E. Saarakkala, G. Pellegrino, and R. Bojoi, "Sensorless self-commissioning of synchronous reluctance motors at standstill without rotor locking," *IEEE Trans. Ind. Appl.*, May/June 2017.
- [26] R. P. Brent, *Algorithms for minimization without derivatives*. Mineola, NY: Dover Publ., 2013.
- [27] M. J. D. Powell, "An efficient method for finding the minimum of a function of several variables without calculating derivatives," *The Comput. J.*, vol. 7, no. 2, pp. 155–162, Jan. 1964.